Author(s): Kemppainen, Erno & Halme, Janne & Hansen, Ole & Seger, Brian & Lund, Peter D.

Title: Two-phase model of hydrogen transport to optimize nanoparticle catalyst loading for hydrogen evolution reaction

Year: 2016

Version: Post print

Please cite the original version:

Kemppainen, Erno & Halme, Janne & Hansen, Ole & Seger, Brian & Lund, Peter D. 2016. Two-phase model of hydrogen transport to optimize nanoparticle catalyst loading for hydrogen evolution reaction. International Journal of Hydrogen Energy. Volume 41, Issue 18. 7568-7581. ISSN 0360-3199 (printed). DOI: 10.1016/j.ijhydene.2015.12.207.

Two-phase model of hydrogen transport to optimize nanoparticle catalyst loading for hydrogen evolution reaction

Erno Kemppainen[a,*], Janne Halme[a], Ole Hansen[b], Brian Seger[c], Peter D. Lund[a]

[a]Aalto University, School of Science, Department of Applied Physics, P.O. Box 15100, FI-00076 Aalto, Espoo, Finland.

[b]Department of Micro- and Nanotechnology, Technical University of Denmark, DK-2800, Denmark.

[c]Center for Individual Nanoparticle Functionality, Department of Physics, Technical University of Denmark, DK-2800, Denmark.

[*]Corresponding author. Tel.: +358 50 409 4907. E-mail address: erno.kemppainen@aalto.fi

Abstract

With electrocatalysts it is important to be able to distinguish between the effects of mass transport and reaction kinetics on the performance of the catalyst. When the hydrogen evolution reaction (HER) is considered, an additional and often neglected detail of mass transport in liquid is the evolution and transport of gaseous H_2, since HER leads to the continuous formation of H_2 bubbles near the electrode. We present a numerical model that includes the transport of both gaseous and dissolved H_2, as well as mass exchange between them, and combine it with a kinetic model of HER at platinum (Pt) nanoparticle electrodes. We study the effect of the diffusion layer thickness and H_2 dissolution rate constant on the importance of gaseous transport, and the effect of equilibrium hydrogen coverage and Pt loading on the kinetic and mass transport overpotentials. Gaseous transport becomes significant when the gas volume fraction is sufficiently high to facilitate H_2 transfer to bubbles within a distance shorter than the diffusion layer thickness. At current densities below about 40 mA/cm^2 the model reduces to an analytical approximation that has characteristics similar to the diffusion of H_2. At higher current densities the increase in the gas volume fraction makes the H_2 surface concentration nonlinear with respect to the current density. Compared to the typical diffusion layer model, our model is an extension that allows more detailed studies of reaction kinetics and mass transport in the electrolyte and the effects of gas bubbles on them.

Keywords

hydrogen evolution reaction, mass transport, gas transport, platinum

1. Introduction

The production of hydrogen by the electrolysis of water could enable the storage of large amounts of solar energy over long time periods. Both solar cells connected to a separate electrolyzer and integrated devices, such as photoelectrochemical cells, could accomplish this at high efficiency [1]. While the integrated devices could benefit from their smaller number of components and lower current density at the electrodes, they are also technically more challenging than connecting a solar panel to an electrolyzer [2,3].

One of the challenges has been to find efficient, stable and cheap catalyst materials. The total reaction of the electrolysis consists of two half-reactions: the oxygen evolution reaction (OER) and the hydrogen evolution reaction (HER). Several catalyst materials have been studied for both reactions, but so far no HER catalyst has shown a performance comparable to that of platinum (Pt) [4,5]. In fact, the charge

transfer kinetics of HER on Pt are so fast that the total overpotential comes almost entirely from mass transport losses, which are consequently sometimes mistaken for reaction kinetics [6–9]. Therefore, understanding the effects of mass transport on the total reaction overpotential, so that they can be reliably distinguished from the kinetics of the charge transfer reactions, is important in order to avoid misinterpretations of measurement results, since the kinetics are the primary focus of attention in performance optimization and mechanistic studies of new HER catalysts.

In our recent feasibility study of ultra-low Pt loadings for use in photoelectrochemical H_2 production we combined experiments with numerical simulations to determine the minimum Pt loading necessary to drive HER in an integrated photoelectrolysis cell [10]. The numerical simulations agreed well with the experiments and showed that Pt loading as low as 100 ng cm^{-2} is enough to drive HER at a 10 mA cm^{-2} current density and a 50 mV overpotential [10]. While this already demonstrated the feasibility of ultra-low Pt loadings, the simulation results also clearly confirmed mass transport effects as the main factor limiting the performance of Pt-based photocathodes, which calls for further attention to this topic.

In this article we develop the single-particle model used in [10] to provide a more detailed description of H_2 mass transport at the photocathode. For the sake of simplicity, H_2 transport in gaseous form was excluded from the previous version of the model [10], because simulations with the more detailed model presented here had shown that, at the current densities generated by un-concentrated sunlight, H_2 mass transport appears similar to diffusion and can therefore be accurately treated by considering only dissolved H_2. Here, we report the model in its extended version that also takes into account gaseous H_2, as well as the dissolution kinetics between the gaseous H_2 in the bubbles and the dissolved molecular H_2 in the liquid phase.

Describing mass transport as a diffusive process is very common, because with some measurement setups (e.g., nano- and microelectrodes [11,12]) mass transport is indeed diffusive, and in other cases, such as with rotating disc electrodes (RDEs)[13], as long as the surface concentration depends linearly on the current density, the surface concentration and mass transport limitation can be described with diffusion, regardless of the actual mass transport process.

Our mass transport model describes both H_2 gas bubbles and H_2 dissolved in water as individual molecules. This is a worthwhile detail to pay attention to because experiments indicate that only the hydrated H_2 molecules in liquid can react at the electrode, whereas the gaseous H_2 is only a passive spectator of the electrode reactions, although most of the H_2 in water actually exists in the gaseous form (bubbles) [14]. When H_2 is generated, these nanobubbles (diameter ≈ 440 nm [14]) act as the nucleation centers for the growth of bubbles [15]. Moreover, it has been observed that increasing the amount of gas bubbles in liquid electrolyte may enhance mass transport, i.e., reduce the thickness of the diffusion layer [16]. Therefore, it is important for a detailed description of mass transport to consider both hydrated molecules and gas, as well as the dissolvation kinetics of H_2 between the liquid and gaseous phases.

Our model is an attempt to describe the effects of the H_2 bubbles on the mass transport within the diffusion layer methodology. Practical simulations often use the diffusion layer approximation because of its simplicity and relatively good accuracy when its thickness is sized correctly. However, with gas bubbles the mass transport of H_2 varies with the current density [16], and therefore the diffusion layer thickness would also need to be adjusted. Several models for the effect of the bubbles on mass transport exist, but they may be quite elaborate [17]. The purpose of our model is to formulate a simple mass transport model that would consistently take the effects of the gas bubbles into account, so that an accurate estimate of the mass transport near equilibrium together with the dynamics of the mass transfer

from the liquid to the bubbles would correctly adjust the overall mass transport conditions to the current density.

Although our model has to be solved numerically, we also develop a simplified version of it that can be solved analytically. Later we will discuss the properties of these models, with most of the attention being paid to a comparison between the numerical simulations and the analytical approximation to study the validity of the simplified model compared with the full numerical model. Since the diffusion of H_2 molecules is a typical approximation for their mass transport and our model is based on the diffusion layer approximation, we also discuss the properties of our model in comparison with the pure diffusional transport of a single chemical species. We also discuss details of the reaction kinetics, especially how the hydrogen coverage of the catalyst affects its current-overpotential curve.

The insights obtained in this study help to provide an understanding of the details of H_2 transport in liquid and the role of the related properties. Although the model assumes a low gas concentration, it serves as a step towards including gas bubbles and their interactions with the liquid electrolyte in the mass transport models used for performance modeling and the simulation of photoelectrochemical devices.

2. Model of the reaction kinetics and mass transport

In this section we describe our model of HER reaction kinetics and mass transport. Our model of the HER reaction kinetics is based on an earlier model by Wang et al. [18] and was described in detail in our earlier article[10], so here we discuss only its essential parts. The most important difference between our model and theirs is that we consider the effect of mass transport on all concentrations and the surface hydrogen coverage, whereas in the model of Wang et al. proton transport and the effect of mass transport on the hydrogen coverage were neglected. The mass transport model is described in more detail, as it is the focus of this article. In this section we both describe the mass transport model and discuss its central characteristics that can be found from an approximate analytical solution to the model.

2.1. Model geometry

We perform the simulations using the diffusional domain approach [19,20], considering the operation of a single Pt nanoparticle (highlighted in red in Figure 1A) in cylindrical geometry. The radius of the simulation cell (light yellow circle) is such that the mass of the Pt particle divided by the area of the cross-section circle is equal to the simulated Pt loading. We assumed a 5 nm diameter in all the simulations. A 2.5-nm-thick smooth Pt layer covering the electrode surface (a protective TiO_2 coating of a silicon solar cell), and simulated using a simulation cell with a radius of 50 nm provided a point of comparison to electrodes fully covered with Pt. This reference case is later referred to as “flat Pt” and it is also useful for theoretical considerations, because it corresponds to the one-dimensional limit of the simulated system.

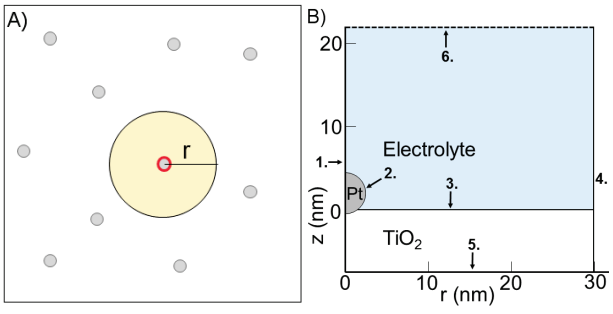

Figure 1. A) Scheme of the diffusion domain unit cell (yellow disk) for 100 ng/cm^2 Pt loading (r ≈ 20 nm) with a single Pt particle in the center. B) Close-up view of the simulation geometry near the electrode surface (Pt loading 50 ng/cm^2). The boundaries 1.-6. are described in the text.

The interfaces and boundaries of the simulation cell are numbered in the scheme in Figure 1B. The symmetry axis is indicated with 1. and the outer edge of the simulation cell with 4. The HER/HOR reaction occurs at the Pt surface (2.) and the exposed surface of the TiO_2 substrate (3.) is inert. Note that the scheme is a close-up view near the catalyst particle: the bulk electrolyte boundary (6.) and the electrical contact of the TiO_2 substrate (5.) are actually outside and much farther from the electrode-electrolyte interface at the opposite ends of the cylindrical simulation cell. The distance between the electrode surface and the bulk electrolyte boundary is called the diffusion layer thickness (Z_b). We assume that the electrolyte is 1 M perchloric acid ($HClO_4$).

The simulations were performed with Comsol Multiphysics (version 5.0). All simulations were run for a simulation time of 20 seconds to ensure convergence to a steady state. The proton concentration profiles needed at most about 10 s to converge to a steady state. Both the current density and H_2 concentration typically converged much earlier, because the dissolution kinetics made the H_2 mass transport faster than pure diffusion and the mass transport losses mostly corresponded to the H_2 concentration. The simulation parameters are given as an appendix (Appendix, Table A.1). Most of the parameters and their values are the same as those that were used earlier[10]; however, there are seven new parameters as a result of the addition of the gas bubbles to the model.

2.2. Reaction kinetics of hydrogen evolution on Pt

The total reaction is

$$2\,H^+ + 2e^- \rightleftarrows H_2 \tag{1}$$

The reaction proceeds through partial reactions:

$$H^+ + e^- \rightleftarrows H_{ad} \quad \text{(Volmer)} \tag{2a}$$

$$H^+ + e^- + H_{ad} \rightleftarrows H_2 \quad \text{(Heyrovsky)} \tag{2b}$$

$$2H_{ad} \rightleftarrows H_2 \quad \text{(Tafel)} \tag{2c}$$

From these, Volmer-Tafel (V-T) and Volmer-Heyrovsky (V-H) mechanisms can be constructed. We assume that the reaction proceeds via the V-T mechanism with Volmer as the rate-limiting step (RLS), as recent results indicate [8]. Because the Heyrovsky step is neglected, the total current density corresponds to the rate ν_V of the Volmer reaction:

$$i_V = q_e N_A \nu_V = i_{0V}\left[\frac{\theta}{\theta^0} e^{\frac{\eta_{sl}}{2}} - \frac{C_{H^+}}{C^0_{H^+}}\left(\frac{1-\theta}{1-\theta^0}\right) e^{-\frac{\eta_{sl}}{2}}\right] \tag{3a}$$

$$\eta_{sl} = \frac{q_e}{k_B T}\left(V_s - (V_l + V_0)\right) \tag{3b}$$

V_0 is the thermodynamic potential of the reaction at the reference concentrations (denoted with 0 in superscript), i.e., 0 V vs RHE, the electrostatic potential in the electrolyte at the electrode surface is V_l and the potential of the electrode is V_s. The total overpotential of the simulations is the electric potential applied to the TiO_2 substrate 100 nm from the electrolyte interface (5. in Figure 1). However, the ohmic losses in the substrate were negligible, so the total overpotential is approximately equal to the electric potential at the Pt surface (2. in Figure 1). The hydrogen coverage of Pt is marked with θ and the proton

concentration at the surface with c_{H^+}. The exchange current density of the Volmer step is i_{0V}, q_e is the elementary charge, N_A the Avogadro's number, k_B the Boltzmann constant and T the temperature in Kelvins. The symmetry factor of both the Volmer and Heyrovsky steps is commonly accepted to be ½.

The Tafel step affects the current density through the surface coverage θ: in a steady state the coverage does not change over time, so the coverage must increase with the current density to allow the H_2 production rate (Tafel rate) to be equal to the proton adsorption rate (Volmer rate). This assumption allows us to derive a quadratic equation of $y = \theta/\theta^0$ to solve the coverage [10,18]:

$$Ay^2 + By + C = 0 \tag{4a}$$

$$\theta = \theta^0 y = \theta^0 \frac{-B+\sqrt{B^2-4AC}}{2A} \tag{4b}$$

The positive root is chosen, because it yields y=1 at η=0 (when c_i=c_i^0 for both protons and H_2). The terms *A, B* and *C* are

$$A = 2r_T\left[(1-\theta^0)^2 - (\theta^0)^2\frac{C_{H_2}}{C^0_{H_2}}\right] \tag{4c}$$

$$B = 4r_T\theta^0\frac{C_{H_2}}{C^0_{H_2}} + e^{\frac{\eta_{sl}}{2}}(1-\theta^0)\left(r_H\frac{C_{H_2}}{C^0_{H_2}}\theta^0 + 1 - \theta^0\right) + e^{-\frac{\eta_{sl}}{2}}(1-\theta^0)\frac{C_{H^+}}{C^0_{H^+}}[r_H(1-\theta^0)+\theta^0] \tag{4d}$$

$$C = -2r_T\frac{C_{H_2}}{C^0_{H_2}} - r_H(1-\theta^0)\frac{C_{H_2}}{C^0_{H_2}}e^{\frac{\eta_{sl}}{2}} - (1-\theta^0)\frac{C_{H^+}}{C^0_{H^+}}e^{-\frac{\eta_{sl}}{2}} \tag{4e}$$

The ratios of the exchange rates of the Tafel and Heyrovsky steps to the Volmer step are marked with r_T (= v_{0T}/v_{0V}) and r_H (= v_{0H}/v_{0V}), respectively. These relations link the surface coverage with surface concentrations and the total overpotential. Details about the derivation of these equations are given elsewhere [10,18]. Note that in equation (4e) we have corrected a typographical error that appeared in the same equation in the SI of our earlier publication [10].

2.3. Mass transport overpotential

The mass transport overpotential is the sum of the electrostatic potential V_l and the Nernst potential difference between the catalyst surface and the bulk electrolyte.

$$\eta_{MT} = V_l + \frac{k_B T}{q_e}\left(\ln\left(\frac{c_{H^+}}{c^0_{H^+}}\right) - \frac{1}{2}\ln\left(\frac{c_{H_2}}{c^0_{H_2}}\right)\right) \tag{5}$$

Although it is known that H_2 transport can cause an overpotential, whose Tafel slope resembles the situation with the Tafel step as the RLS, this is often not considered when analyzing results [6,8], and the mass transport losses are interpreted as reaction kinetics. More detailed discussion is available elsewhere [8,10,21]. The main conclusion of these studies regarding mass transport losses is that when the kinetic overpotential is negligible and the current density is small compared to the limiting current density of HER, the overpotential corresponds to the H_2 transport losses and its Tafel slope is about 30 mV/decade (at room temperature):

$$i \approx i_{lim,\mathrm{HOR}}\left(1 - e^{-2\eta'}\right) \tag{6a}$$

$$\eta' = \frac{q_e}{k_B T}(V_s - V_0) \tag{6b}$$

The potential V_l is neglected here, because electroneutrality means that the potential remains small.

2.4. Transport of ions and molecules in the electrolyte

The model used here is for the most parts the same as used earlier [10], apart from the key differences associated with the inclusion of gaseous H_2 in the mass transport model. As already mentioned, this refinement of the model seems necessary for a full, accurate description, since most of the H_2 in the electrolyte is known to be present in the form of small gas bubbles, whereas only hydrated H_2 molecules in the liquid participate in the electrode reactions [14].

Because the gas bubbles occupy a fraction of the electrolyte volume (f_g), the flux densities ($\boldsymbol{j}_n$) of the ions and molecules in the liquid are reduced by the same fraction. As a result, the transport and continuity equations for species n with the concentration c_n become

$$\boldsymbol{j}_n = -f_l D_n \nabla c_n - z_n f_l \mu_n c_n \nabla V_l + c_n \boldsymbol{v_l} \approx -f_l D_n \left(\nabla c_n - \frac{z_n q_e}{k_B T} c_n \nabla V_l \right) \tag{7a}$$

$$\frac{\partial c_n}{\partial t} = -\nabla \cdot \boldsymbol{j}_n + R_n \approx D_n \nabla \cdot \left[f_l \left(\nabla c_n - \frac{z_n q_e}{k_B T} c_n \nabla V_l \right) \right] + R_n \tag{7b}$$

where the fraction of the total volume occupied by the liquid, i.e., the liquid volume fraction, is f_l (= 1 - f_g). Unfortunately, because of software limitations, the liquid fraction could not be properly implemented in practice when the liquid velocity ($\boldsymbol{v_l}$) was included in the model as in equation 7a. However, the liquid velocity was negligible in the simulations, meaning that the convective transport term ($c_n \boldsymbol{v_l}$) could be omitted from the analysis and simplified model. With this approximation, the end result is that the liquid volume fraction scales the bulk diffusion coefficient (D_n) locally. HER/HOR at the Pt surface (2. in Figure 1) is described as a flux density boundary condition for protons and dissolved H_2. The mass exchange with H_2 gas is an additional source term for the dissolved H_2 molecules (Section 2.6). For perchlorate ions $R_n = 0$.

Electroneutrality is assumed, so the concentrations of protons and perchlorate ions are equal, but their mobility difference affects the transport of both species in a similar manner to an electric field[22]

$$\nabla V_l = -\frac{k_B T}{q_e} \left[\left(\frac{D_{H^+} - D_{ClO_4^-}}{D_{H^+} + D_{ClO_4^-}} \right) \nabla \left(\ln \frac{c_{H^+}}{c_{H^+}^0} \right) - \frac{\boldsymbol{i}}{q_e N_A f_l c_{H^+} \left(D_{H^+} + D_{ClO_4^-} \right)} \right] \tag{8}$$

The second term of the potential gradient corresponds to the resistive losses in the electrolyte and in it $\boldsymbol{i}$ is the current density vector in the electrolyte, not the current density at the catalyst surface (equation (3a)). It is assumed that in the bulk electrolyte $V_l = 0$ and the potential at the catalyst surface (equation (3b)) is this gradient integrated over the diffusion layer.

Because gas bubbles also occupy part of the total volume at the catalyst surface, the actual current density on the catalyst surface (i) corresponds to the Volmer current density multiplied by the fraction of the catalyst surface in contact with the liquid.

$$i = f_l i_V \tag{9}$$

In the earlier article [10] gas bubbles were not included in the model. The present extended model reduces to the earlier model by setting $f_l = 1$ in all the equations presented here (i.e., no gas present), and removing the source term R_n from equation 7b (i.e., no H_2 mass exchange with the gas bubbles). The kinetic model that describes the reactions at the catalyst surface is identical to the previous version of the model [10]. In the following sections (2.5-2.7) we present our gas transport model and discuss some of its basic properties.

2.5. Liquid and gas flow

We model the movement of liquid and gas with the Laminar Bubbly Flow mode of the computational fluid dynamics module of Comsol Multiphysics (version 5.0) without turbulence, and assuming a low gas concentration. Because we simulate the operation of a single catalyst particle in a (cylindrical) unit cell, whose cross-section is smaller than the cross-section of the bubbles, we cannot explicitly simulate the fluid transport in the model, but need to use a simplified description.

The gas concentration is assumed to be small, so its contribution to the momentum transport of the mixture is assumed to be negligible.

$$f_l \rho_l \frac{\partial \boldsymbol{v_l}}{\partial t} + f_l \rho_l \boldsymbol{v_l} \cdot \nabla \boldsymbol{v_l} = \nabla \cdot [-p\boldsymbol{I} + f_l \mu_l (\nabla \boldsymbol{v_l} + (\nabla \boldsymbol{v_l})^T)] \quad (10)$$

The pressure is p and $\boldsymbol{I}$ is the identity matrix. The second term inside the brackets ($f_l\mu_l(\nabla \boldsymbol{v_l} + (\nabla \boldsymbol{v_l})^T$) is the viscous stress tensor. There are no external forces ($\boldsymbol{F}=\boldsymbol{0}$) and gravity was neglected ($\boldsymbol{g}=\boldsymbol{0}$).

The liquid is assumed to be incompressible:

$$\nabla \cdot \boldsymbol{v}_l = 0 \quad (11)$$

The transport of gaseous H_2 is solved from the mass continuity equation:

$$\frac{\partial f_g \rho_g}{\partial t} = -\nabla \cdot \left(f_g \rho_g \boldsymbol{v}_g\right) - m_{gl} \quad (12)$$

The product of the volume fraction of gas (f_g) and its density (ρ_g) is called the effective density of gas. The mass transfer between gas and hydrated H_2 (m_{gl}) depends on the local concentration and effective density (details in the next section). The gas flux density is

$$\boldsymbol{j_g} = f_g \rho_g \boldsymbol{v}_g \quad (13)$$

and the velocity of the gas ($\boldsymbol{v}_g$) is the sum of the velocity of the liquid ($\boldsymbol{v}_l$) and the drift velocity of the bubbles with respect to the surrounding liquid ($\boldsymbol{v}_{\text{drift}}$) that corresponds to their diffusion and depends on the properties of the surrounding liquid:

$$\boldsymbol{v}_g = \boldsymbol{v}_l + \boldsymbol{v}_{\text{drift}} \quad (14a)$$

$$\boldsymbol{v}_{\text{drift}} = -\frac{\mu_l}{\rho_l} \frac{\nabla f_g}{f_g} \quad (14b)$$

The density of the liquid is ρ_l (water at 298.15 K, 997.08 kg/m^3) and its dynamic viscosity is μ_l (9×10^{-4} Pa·s, yielding the kinematic viscosity $\mu_l/\rho_l \approx 9.0\times10^{-7}$ m^2/s).

The boundary conditions are as follows: the electrode interfaces (2. and 3. in Figure 1) are treated as walls with no slip for liquid and zero flux density for gas, i.e.,

$$\boldsymbol{v}_l = \boldsymbol{0} \quad (15a)$$

$$-\boldsymbol{n} \cdot \boldsymbol{j_g} = 0 \quad (15b)$$

The vector $\boldsymbol{n}$ is the normal vector of the surface or boundary in question. At both the bulk electrolyte interface (6.) and the outer edge of the unit cell (4.) the boundary condition for the liquid is a set pressure:

$$p = p_0 \quad (16)$$

At the bulk electrolyte interface the effective density of the gas corresponds to the equilibrium concentration of H_2 in water under H_2 pressure of 1 bar (0.77 mM), i.e., 0.0015518 kg/m^3, and at the outer edge of the unit cell the gas flux density is set to zero (eq. (15b)).

2.6. Mass exchange of H_2 between gas and liquid phases

When the pressure of H_2 is 1 bar, the corresponding equilibrium concentration of H_2 in water is 0.77 mM. However, most of this is apparently in the form of submicron (diameter ≈ 440 nm) gas bubbles that also serve as the nucleation centers for bubble growth, when H_2 is produced, and less than 10% is in hydrated form that may react at the electrodes [14,15]. We assume that in equilibrium the effective density of the gas corresponds to a concentration of 0.77 mM and the concentration of hydrated H_2 molecules is one tenth of that, i.e., 0.077 mM. We use Henry's law to describe the equilibrium between the gas bubbles (p) and dissolved H_2 (c):

$$c_{H_2}^0 = \frac{p_{H_2}^0}{k_{H,H_2}} \tag{17}$$

Since we assume that in equilibrium the H_2 pressure is 1 bar and the concentration of dissolved H_2 is 0.077 mM, equation (17) yields a coefficient $k_{H,H2}$ = 12990 bar/M. All the simulations were performed at a temperature of 298.15 K, so the temperature dependence of the coefficient could be neglected. The rate of mass exchange between the gas and dissolved phase depends on the surface area of the gas bubbles. The mass exchange rate per volume is[23]

$$m_{gl} = ak_{diss}\left(\frac{p_{H_2}}{k_{H,H_2}} - c_{H_2}\right)M_{H_2} \tag{18}$$

where a is the bubble surface area per unit volume (m^2/m^3), M_{H_2} the molar mass of H_2 and k_{diss} the rate constant for the dissolution process (0.4 mm/s [14]). Negative mass exchange rates correspond to dissolved molecules forming gas and positive ones to gas dissolving into the liquid. When the volume fraction of gas in the liquid-gas mixture is f_g and the diameter of the bubbles is d_b, the total number of bubbles per volume, n_b, is

$$n_b = \frac{f_g}{V_b} = \frac{f_g}{\frac{4}{3}\pi\left(\frac{d_b}{2}\right)^3} \tag{19}$$

The surface area per volume is the number of bubbles per volume multiplied by the surface area of a single bubble. We assume spherical bubbles with a constant diameter (d_b = 440 nm [14])

$$a = n_b 4\pi\left(\frac{d_b}{2}\right)^2 = \frac{6f_g}{d_b} \tag{20}$$

Inserting this into the original rate expression (eq. (18)) gives

$$m_{gl} = k_{diss}\left(\frac{p_{H_2}}{k_{H,H_2}} - c_{H_2}\right)\frac{6f_g M_{H_2}}{d_b} \tag{21}$$

This approximation does not take into account the different sizes of the bubbles or their growth, but assumes an average diameter that describes the overall situation for the mass exchange. Therefore the model best describes a situation where the H_2 concentration may differ from the saturation concentration, but the individual bubbles and the gas volume fraction are small.

2.7. Simplified mass exchange – transport model

The mass exchange between dissolved H_2 and gas bubbles may increase the mass transport rate of dissolved H_2 compared to a situation with only dissolved H_2. For HER the gaseous H_2 acts as a hydrogen sink and for HOR as its source, analogously to a bulk electrolyte, but extended over the whole diffusion layer thickness. To our knowledge, the coupled H_2 transport problem (equations (7b), (12) and (21), $R_{gl} = m_{gl}/M_{H2}$) cannot be solved in closed form, and analytical expressions require simplifications. Figure 2 shows the volume fraction of the gas bubbles at the electrode surface as a function of the current density from the exact numerical solution (flat Pt). At low current densities the volume fraction at the electrode is constant, i.e., independent of both the current density and diffusion layer thickness, and equal to the volume fraction in the bulk electrolyte. This immediately shows that, to a good approximation, we can also assume the volume fraction to be independent of the position within the simulation cell, provided that the current density is sufficiently low. The highest current density at which the approximation can be considered good depends on the diffusion layer thickness (and on the parameters that affect gas diffusivity), as will be discussed later in more detail. We also note that, although it is not readily visible in Figure 2, the gas volume fraction increases linearly with the current density up to a 10% fraction, but above this limit the rate of increase decreases. However, with all the simulation parameter values used here, this occurs only at very high current densities (> 1 A/cm^2) that could be found only in (dark) electrolysis cells or in photoelectrolysis cells that use sunlight concentrated by a factor of 100 or more.

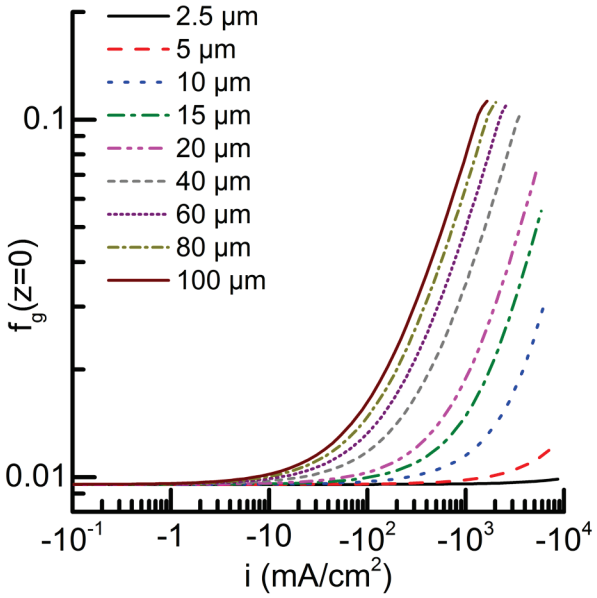

Figure 2. Gas volume fraction at the electrode surface as a function of the current density for a smooth (flat) Pt surface and different diffusion layer thicknesses.

When we assume that the pressure and gas volume fraction are constant (and liquid velocity negligible) over the entire diffusion layer thickness and replace the liquid volume fraction with $1\text{-}f_g$ ($f_l+f_g=1$), we get a linear differential equation for the concentration of the dissolved hydrogen:

$$(1-f_g)D_{H_2}\frac{\partial^2 c_{H_2}}{\partial z^2} + k_{diss}\left(\frac{p_{H_2}}{k_{H,H_2}} - c_{H_2}\right)\frac{6f_g}{d_b} = 0 \qquad (22)$$

This equation can be solved analytically and the resulting concentration profile consists of exponential functions of the distance from the Pt surface. When the concentration at the bulk electrolyte boundary (z =

Z_b) is equal to the bulk concentration, and the flux at the electrode surface ($z = 0$) corresponds to the current density, we get

$$c_{H_2}(z) = c_{H_2}^0 + \frac{iL}{2FD_{H_2}}\left(\frac{\sinh\left(\frac{z}{L}\right) - \sinh\left(\frac{2Z_b - z}{L}\right)}{\cosh\left(\frac{2Z_b}{L}\right)+1}\right) \tag{23a}$$

$$L = \sqrt{\frac{d_b D_{H_2}}{6k_{diss}}\left(\frac{1}{f_g} - 1\right)} \tag{23b}$$

If $Z_b >> L$, the concentration profile can be simplified to

$$c_{H_2}(z) \approx c_{H_2}^0 - \frac{iL}{2FD_{H_2}} e^{-\frac{z}{L}} \tag{23c}$$

The concentration in the bulk electrolyte is c_{H2}^0 ($=p_{H2}/k_{H,H2}$), corresponding to the pressure of 1 bar in the bulk, Z_b is the thickness of the diffusion layer and L is the diffusion length of the dissolved H_2 molecules. Note that the interpretation of L is analogous to the interpretation of the diffusion length of electrons or holes in a semiconductor: it is a characteristic distance that the diffusing species (here dissolved H_2 molecules) are able to move (on average) by diffusion before they are consumed by reactions (here transfer to H_2 bubbles). The rate constant k_{diss} (or rather $k_{diss}f_g/d_b$) is an important factor in determining whether the mass exchange or diffusion layer thickness is more significant for mass transport: k_{diss}=0 obviously corresponds to pure diffusional mass transport that is fully determined by the diffusion layer thickness (Z_b). By contrast, a large rate constant yields a short diffusion length ($Z_b >> L$), meaning that the H_2 that is produced will form gas bubbles rapidly near the catalyst, and for most of the diffusion layer thickness H_2 transport proceeds in gas phase (see also Figure 4). Because in this simplified model the gas volume fraction is assumed to be constant, the diffusion length is also constant. In the full numerical model, where the gas volume is allowed to vary as a function of position, the concept of the diffusion length of the dissolved H_2 is less apparent, but can nevertheless be considered as a locally varying characteristic of the competition between diffusion and reaction that depends on the local gas volume fraction according to eq. (23b).

With the values that we used in the simulations (d_b=440 nm, k_{diss}=0.4 mm/s, D_{H2}=5.11×10^{-5} cm^2/s, Table A.1), the diffusion length for 0.95% bulk gas volume fraction is about 9.9 µm, and 6.8 µm for a 2% volume fraction. Its value decreases monotonically as a function of f_g, meaning that increasing the gas volume fraction will always yield faster mass transfer kinetics because of a larger bubble surface area per unit volume. At low volume fractions this is probably true, but when the volume fraction becomes large, this approximation could yield too high rates, because most probably the bubbles will grow when the gas volume fraction increases, reducing the surface area. We expect this behavior to be somewhat similar to how some other bubble transport models based on gas diffusion at low concentrations overestimate the mass transport rate compared to more detailed models when the gas volume fraction increases[17].

By inserting $z = 0$ into equation (23a), we get an analytical expression for the surface concentration of the dissolved H_2.

$$c_{H_2}(z = 0) = c_{H_2}^0 - \frac{iL\tanh\left(\frac{Z_b}{L}\right)}{2FD_{H_2}} \tag{24a}$$

Because in our approximation L is constant, we can express the dependence of the surface concentration on the current density formally in a similar way to the case of diffusive transport without bulk reactions,

i.e., in terms of two characteristic parameters: the bulk concentration $c_{H_2}^0$ and the limiting current density $i_{\mathrm{lim,HOR}}$, which depends on the effective diffusion layer thickness $Z_{\mathrm{b,eff}}$, which in turn is a function of L (eq 23b).

$$\frac{c_{H_2}(z=0)}{c_{H_2}^0} = 1 - \frac{i}{i_{lim,HOR}} \tag{24b}$$

$$i_{lim,HOR} = \frac{2FD_{H_2}c_{H_2}^0}{Z_{b,eff}} \tag{24c}$$

$$Z_{b,eff} = L\tanh\left(\frac{Z_b}{L}\right) \tag{24d}$$

Eq (24d) shows that if the true diffusion layer thickness Z_b is much larger than L, the effective diffusion layer thickness $Z_{\mathrm{b,eff}}$ is approximately equal to L, and the limiting current density corresponds to the dissolution kinetics and mobility of the dissolved molecules, which could be anticipated from the absence of Z_{b} in equation (23c). In this situation all the dissolved H_2 that is produced transfers to the bubbles near the electrode without reaching the bulk electrolyte situated at $z = Z_b$. The limiting current density is then

$$i_{lim,HOR} \approx 2Fc_{H_2}^0\sqrt{\frac{6D_{H_2}k_{diss}}{d_b\left(\frac{1}{f_g}-1\right)}} \tag{25}$$

In the opposite case, where $L >> Z_b$, the transfer to the bubbles is so slow that the dissolved H_2 has enough time to diffuse across the whole diffusion layer, i.e., $Z_{\mathrm{b,eff}} \approx Z_{\mathrm{b}}$, which corresponds to the H_2 mass transport being fully diffusive with only negligible mass exchange between the dissolved molecules and gas bubbles. Note that $i_{\mathrm{lim,HOR}} > 0$ mA/cm^2, i.e., has a positive sign, whereas $i < 0$ mA/cm^2, because we consider HER. In other words, $i_{\mathrm{lim,HOR}}$ does not limit the H_2 production rate, but is merely a characteristic parameter of the diffusion problem (it would limit the H_2 *consumption* rate, though).

Conversely, when we know the current density and surface concentration of H_2, we can calculate the apparent limiting current density of HOR as a function of the current density from equation (24b).

$$i_{lim,HOR} = \frac{i}{1-\frac{c_{H_2}(z=0)}{c_{H_2}^0}} \tag{26}$$

We use this equation to calculate the apparent limiting current density of the full numerical simulations as a function of the current density. This functions as a criterion for the validity of the simplified model: when the calculated limiting current density is constant with respect to the current density, the simplified model is valid, and more generally, the mass transport behaves similarly to diffusion. When the gas volume fraction in our model increases, the effective diffusion layer thickness decreases and the limiting current density increases. At low current densities this is probably not a significant factor, but when the current density and gas volume fraction increase (Figure 2), at some point the surface concentration probably cannot be described with the limiting current density that corresponds to the equilibrium volume fraction.

Figure 3 below illustrates this by showing a comparison of the concentration profiles of the full numerical simulations (solid lines) with the simplified model (dashed lines, equations (23a) and (23b) with the bulk gas volume fraction). The diffusion layer thickness Z_{b} is 100 µm and the corresponding gas volume fraction in the full simulations can be found from Figure 2. Up to 10 mA/cm^2 there is practically no difference between the solutions, and the gas volume fraction is also only a little higher than its bulk

value. However, at 100 mA/cm^2 the surface gas volume fraction is twice as large as the bulk fraction and at 1 A/cm^2 it is already about 10%, which is more than ten times the bulk value. This difference is also apparent in the concentration profiles in Figure 3. While the simplified solution is relatively close to the full simulation at 100 mA/cm^2, the difference is significant at 1 A/cm^2. Moreover, at 1 A/cm^2 the simplified solution fails to reproduce the increased concentration gradient caused by the increased gas volume fraction and thus the reduced diffusion length. Overall, if only the surface H_2 concentration is needed as a result from the modeling, the simplified model presented here, and therefore also diffusive transport, seems sufficiently accurate up to almost 100 mA/cm^2, as long as the limiting current densities are realistic. This is also why gas phase H_2 transport could safely be omitted from our previous publication, and a simple diffusion model (eq. (7) without mass exchange and $f_l = 1$, and thus also eq. (24b)) was used instead [10]. At higher current densities the surface concentrations of diffusive transport models differ significantly from the numerical simulations with our two-phase transport model.

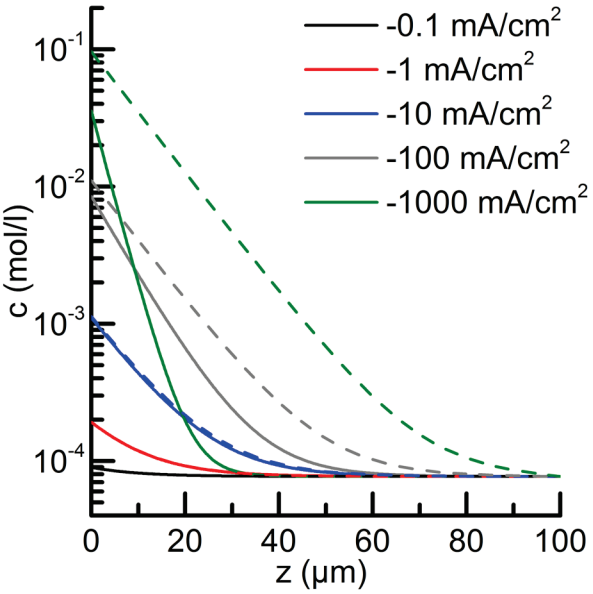

Figure 3. Concentration profiles of dissolved H_2 at different current densities with 100 µm diffusion layer thickness: full numerical solutions (flat Pt, solid lines) and the simplified 1D model (equation (23), dashed lines). The dashed black and red lines are not visible because they overlap with the corresponding solid lines.

The effect of the diffusion layer thickness (Z_b) on flat Pt (1D limit of the model) is illustrated in Figure 4. Figure 4A shows typical concentration profiles of both dissolved and gaseous H_2 at -100 mV vs RHE. Note that the profiles are the full numerical solution of the problem, not the simplified one given by equation (23). The current density is not the same in all cases, but for diffusion layer thicknesses of 15 µm or more it is about -250 mA/cm^2 (Figure 4B). As Figure 4A illustrates, when the diffusion layer thickness is 40 µm or more, the concentration of the dissolved H_2 decreases approximately exponentially at distances less than about 30 µm from the electrode surface (at $z=0$), but the rate varies with the diffusion layer thickness (Z_b), since the gas volume fraction (concentration in Figure 4A) depends on Z_b. By a distance of 60 µm from the electrode surface the H_2 concentration is reduced to its bulk level, even if the bulk electrolyte is farther from the electrode. The concentration of gaseous H_2 changes almost linearly as a function of the distance everywhere, except close to the electrode surface, which is not apparent because of the logarithmic concentration axis. Therefore, the volume fraction is clearly not constant. However,

because its variations were significantly smaller than the variations in the concentration of the dissolved H_2, it could be possible to use equation (23) as an approximation, although not always with the equilibrium gas volume fraction.

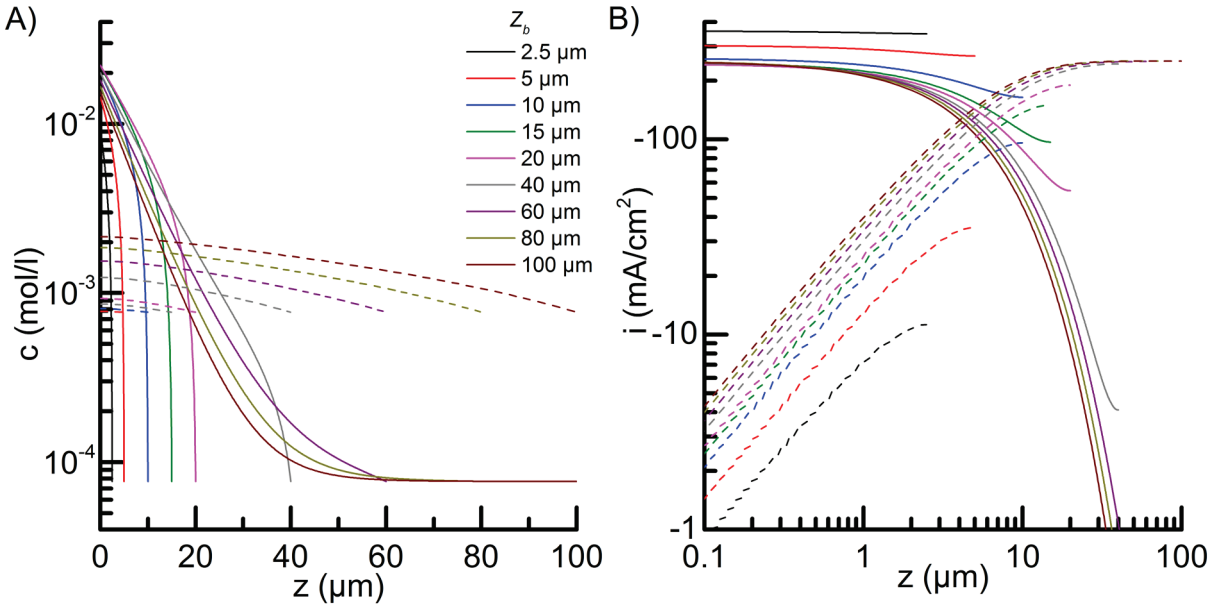

Figure 4. Examples of the behavior of H_2 concentrations in the 1D limit of our model (i.e., flat Pt). A) Numerically solved concentration profiles of dissolved H_2 (solid lines) and gas (dashed lines) for the indicated diffusion layer thicknesses. B) Flux density profiles calculated from the concentration profiles in fig A) converted to current density.

Figure 4B shows the H_2 flux carried by the dissolved molecules and gas bubbles converted to current density ($z = 2$) to accommodate comparison with other figures, where current density is used. As a consequence of the dissolved molecules entering the bubbles, most of the H_2 flux density is carried as gas bubbles at distances of more than approximately 5 µm from the electrode surface, and at a distance of 20 µm the flux density of the dissolved H_2 is negligible compared to the total gas flux density. The exact point, where the gas flux becomes higher than the molecular flux depends on the current density and on the diffusion layer thickness. Slightly surprisingly, increasing the current density at a given diffusion layer thickness brings this point closer to the electrode surface, and increasing the diffusion layer thickness seems to do the same. In both cases the amount of gas near the electrode is increased, which enhances the mass exchange kinetics (see also Figure 5). However, when the diffusion layer thickness was less than 10 µm, mass exchange was not fast enough to shift the majority of the flux density to gaseous H_2 at any current density. Nonetheless, with a diffusion layer thickness of 15 µm the crossing point is already no farther than approximately 7 µm from the electrode (green lines in Figure 4B).

3. Results and Discussion

3.1. Mass transport and total overpotential

In the previous section we illustrated the main features of our model and showed how the complete model differs from the simplified solution. In this section we discuss how bubble transport and formation kinetics affect H_2 transport. This includes both the assumed diffusion layer thickness and the dissolution rate constant. Finally, we also discuss the factors that were neglected in this model and how they could affect the results, and could possibly be included in a more elaborate model.

3.1.1. Gas volume fraction and diffusion layer thickness

Figure 5 shows the diffusion length of the H_2 molecules at the Pt surface as a function of the current density, calculated with equation (23b) from the volume fractions shown in Figure 2. A comparison of Figures 2, 3 and 5 indicates that the failure of the simplified model at high current densities is due to the increased gas volume fraction, which reduces the diffusion length, which can be seen in Figure 3 as the clearly steeper slope of the simulated concentration profile for a current density of 1 A/cm^2. Note that because of the one-to-one relation between L and f_g via equation (23b), Figure 5 conveys essentially the same information as Figure 2, which was already discussed.

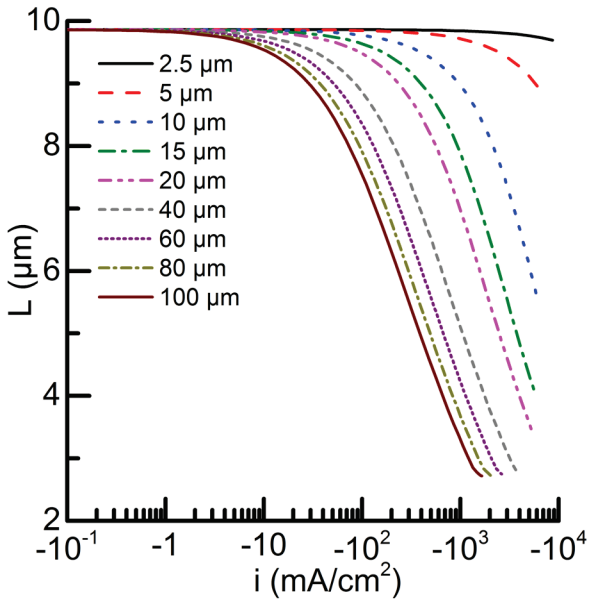

Figure 5. The diffusion length of H_2 molecules at the flat Pt electrode surface calculated from the gas volume fractions in Figure 2 as a function of current density for the indicated values of Z_b.

In addition to the diffusion length, we can calculate the apparent HOR limiting current density from the surface concentration of dissolved H_2 (equation (26)). While the diffusion length describes the concentration profile in the immediate vicinity of the electrode, the limiting current density serves as an indicator of the overall mass transport rate and the behavior of the surface concentration as a function of the current density. As a descriptor of H_2 mass transport, the apparent limiting current density serves two purposes:

1. as mentioned, it is an indicator of the overall H_2 mass transport rate, with higher values corresponding to faster mass transport. Additionally, in the simplified model (and with diffusive transport) the mass transport losses are given approximately by the limiting current density alone (equation (6)), so we can connect it directly to the mass transport overpotential;
2. it allows us easily to determine the current density range, where the simplified model is valid, because in that case the surface concentration is described by a constant limiting current density, similarly to diffusive mass transport. When we see this behavior or deviation from it in the full numerical simulations, it is easy to distinguish between the validity and failure of the simpler model.

Figure 6 shows the apparent HOR limiting current density (A, equation (26)) and mass transport overpotential (B, equation (5)) for the full numerical simulations and indicated diffusion layer

thicknesses. At low current densities all cases can be described with a constant limiting current density, meaning that the simplified model is valid. However, as the current density increases, the apparent limiting current density (equation (25)) also increases, because the increased gas volume fraction enhances the mass exchange kinetics and therefore the removal of H_2 molecules from the electrode surface. Because the gas volume fraction increases continuously, the apparent limiting current density also increases smoothly. A comparison of Figures 2 and 6 indicates that this increase becomes significant when the volume fraction has increased by about 10% to 1.1%, corresponding to a diffusion length a little greater than 9 µm (Figure 5.). This is not apparent from Figure 6A for the thinnest diffusion layers, but the increase would probably also happen in their case at current densities even higher (> 10 A/cm^2) than those encountered in the present simulations.

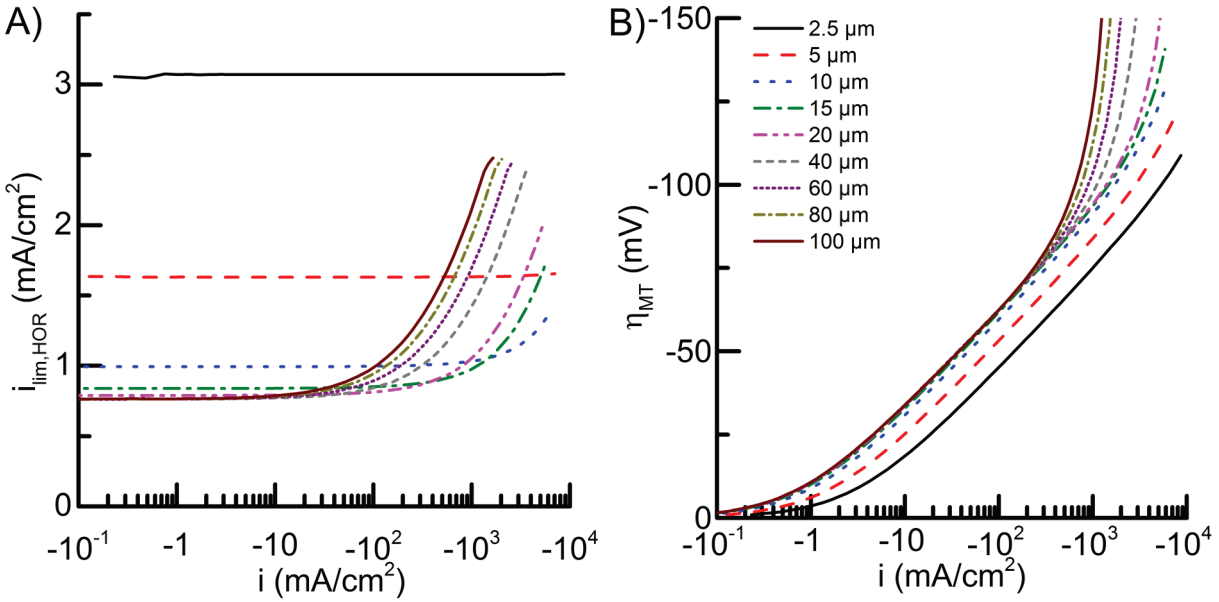

Figure 6. The effect of the diffusion layer thickness (Z_b) on H_2 transport. A) The apparent HOR limiting current density calculated from the surface concentration of H_2 and B) the mass transport losses as a function of current density.

At low current densities $i_{lim,HOR}$ decreases with an increasing diffusion layer thickness Z_b, until it saturates to a nearly constant value that is independent of both the current density and Z_b. The saturation occurs because the dissolved H_2 molecules are transferred to gas bubbles and their concentration will reduce to the bulk value before the bulk electrolyte if Z_b is significantly larger than the diffusion length of the molecules (L). In that case $i_{lim,HOR}$ corresponds only to L (equations (24d) and (25), and Figure 4). The mass transport overpotential follows this behavior at low current densities: first it increases with increasing Z_b but then it saturates to a constant value determined only by L and the current density (equations (6) and (24d)).

At high current densities proton transport also becomes important. This can be seen in Figure 6B as a rapid increase in the mass transport overpotential when the current density approaches the limiting current density of proton transport. This increase becomes significant at current densities above ca. 1 A/cm^2, depending on the Z_b. For example, with Z_b = 100 µm, the effect becomes visible in Figure 6B at ca. 300 mA/cm^2, which is ca. 15% of the HER limiting current density in the same situation (ca. 1.8 A/cm^2). At these higher current densities a thicker diffusion layer always leads to a higher overpotential (Figure 6B),

because unlike the dissolved H_2 that can transfer to the H_2 bubbles, protons always have to be transported through the whole diffusion layer thickness.

The increase in the HOR limiting current density as a function of the current density is in qualitative agreement with published experimental results [16]. The behavior of the gas volume fraction in our simulations also agrees well with experiments on the bubble coverage of electrodes, although our simulated gas volume fractions are smaller than those observed experimentally at the same current density [24]. This could be due to overestimated gas diffusivity, but also other factors that affect the behavior of bubbles at real electrodes.

3.1.2.Mass exchange kinetics

As predicted by the simplified model, variation in the rate constant has similar effects on the H_2 surface concentration to varying $i_{lim,HOR}$ (Figure 7). Indeed, Figure 7B shows that $i_{lim,HOR}$ derived from the simulation results (c_{H2}, square markers) depends on the square root of k_{diss} at current densities less than 10 mA/cm^2, as predicted by equation (25), indicating that the simplified solution is very accurate, at least in the rate constant range under study. It is interesting to note that $i_{lim,HOR}$ starts a rapid increase at around 20 mA/cm^2 regardless of the value of k_{diss}. In other words, k_{diss} simply shifts the curves along the vertical axis in Figure 7A.

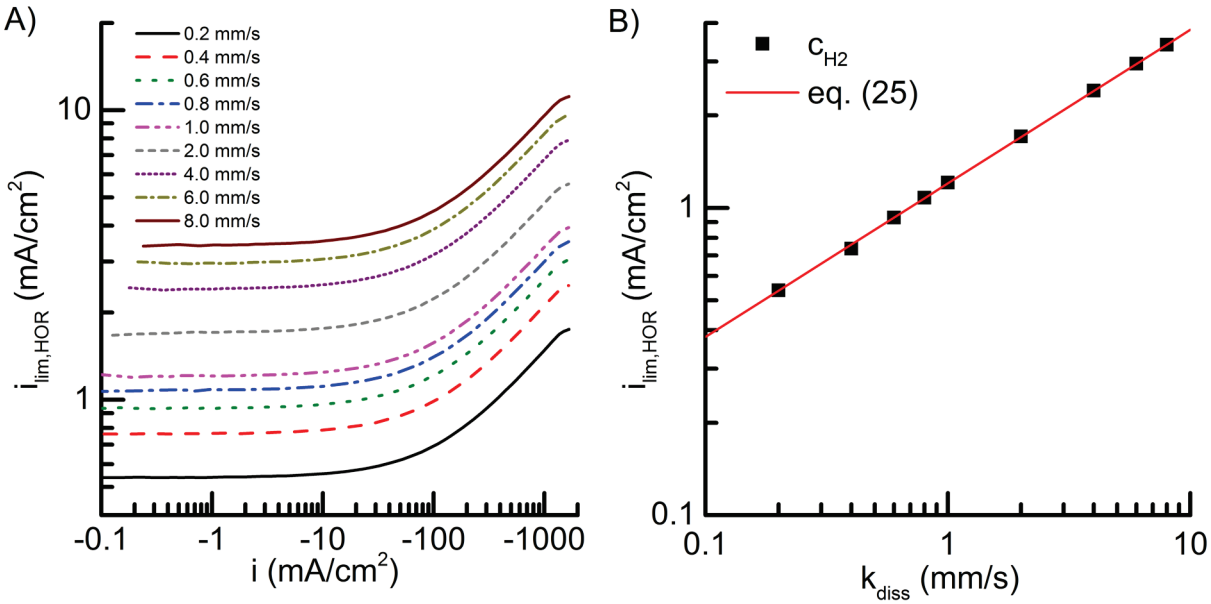

Figure 7. The effect of the mass exchange kinetics on the overall H_2 mass transport with Z_b = 100 µm. A) The apparent limiting current density for different values of k_{diss}. B) The dependence of the apparent limiting current density on the rate constant at low current densities.

The rate constant of the kinetics (k_{diss}) is not the only parameter that affects the kinetics, because the bubble diameter (d_b) also has a similar role in the expression of the mass exchange rate. However, since in our model they both affect only the mass exchange kinetics, we can study the kinetics by varying only a single parameter, here the rate constant. The kinetic rate is inversely proportional to the diameter of the bubble and linearly proportional to the rate constant, so increasing the bubble size would affect the kinetics in a similar way to reducing the rate constant.

3.1.3. Remarks on the limitations of the H_2 transport model

Several factors were excluded from the present model because of their complexity, but may influence the H_2 transport in real devices and therefore deserve a brief discussion, not least because they may provide a way to improve the predictive power of the model with respect to experimental results.

One of them is fluid motion. In practice, our approach limits us to the movement of gas bubbles and its effects. In the present model the gas flux has no effect on the fluxes of ions and molecules in the liquid beyond the local volume fraction, whereas in reality the movement of the bubbles would stir the liquid, which could reduce the effect of the reduced liquid volume fraction. Therefore, it might be possible that a small or moderate amount of gas might even improve the proton transport, and thus increase the apparent HER limiting current density. In our model increasing the gas volume fraction reduces the HER limiting current density, because the total proton flux density is reduced. The current density at which the increase in the volume fraction becomes noticeable also depends on the diffusivity of the gas bubbles, so slower gas movement would correspond to a lower current density, where H_2 transport is no longer described accurately by a constant limiting current density.

Another related factor is the lack of bubble growth. We did not account for the possibility of bubbles growing or coalescing together to form larger bubbles. The increased bubble size would naturally affect the surface area of the bubbles per unit volume, so at least the dissolution kinetics would be affected. The bubble size would probably also affect bubble diffusivity and liquid flow near the bubbles, which could then affect the surface concentrations of protons and H_2.

In practice these effects could be included by, for example, modifying the dependence of the fluxes on the liquid volume fraction and making the bubble radius a function of the gas volume fraction. The problem is then to find the correct functional dependence that can be used.

One important detail that our model most probably describes correctly is that an increase in the amount of gas will eventually reduce the proton supply and active reaction surface area, leading to slower gas formation [25,26]. The balance of the gas and proton transport could determine either an upper limit or a clear peak value of the current density [25]. However, because we saw at most gas volume fractions of about 13 % at current densities almost as high as the HER limiting current density (about 1800 mA/cm^2 for a 100 μm diffusion layer, if the gas volume fraction is neglected), we do not know exactly how our model would behave at the high gas volume fraction limit. Neither do we expect to see significantly higher gas volume fractions at the electrode surface at any bias potential with the simulation parameters used. Therefore, studying the high gas volume fraction range, if such studies are considered reasonable, would require the modification of some of the simulation parameters to allow sufficient H_2 concentrations to develop. We point out, however, that our model is strictly valid only at low gas concentrations and therefore will probably fail in more than one way at higher gas concentrations.

3.2. The effect of catalyst loading

The catalyst loading on the electrode determines the number of reaction sites per electrode area. For a fixed current density per electrode area, increasing the catalyst loading reduces the current density per catalyst surface area, and therefore also the kinetic overpotentials. On the contrary, the mass transport overpotentials arise as a result of the transport of electroactive species in the electrolyte, both in the bulk and near the catalyst particles. It is therefore less obvious how they depend on the number of catalyst particles per electrode area. In our previous study we observed that the mass transport losses at a given current density (per electrode area) are almost independent of the catalyst loading, i.e., changing the

catalyst loading affected only the kinetic overpotential [10]. We show the same observation here with slower mass transport (lower $i_{lim,HOR}$) to illustrate it better.

Figure 8 shows the situation for four Pt loadings ranging from 10 ng/cm^2 to 1000 ng/cm^2 with a diffusion layer thickness of 100 µm ($i_{lim,HOR} \approx 0.77$ mA/cm^2 at low current densities; see, e.g., Figure 7). The reaction kinetics and mass transport are the same in all cases; only the amount of catalyst changes, and with it both the current density per catalyst area and the kinetic overpotential. With very low loadings the current density per catalyst area is high and the kinetic overpotential is large compared with the mass transport losses. In this case the total overpotential mostly corresponds to the kinetic losses, which brings the current-overpotential curve very close to the theoretical limit without mass transport losses, as shown in Figure 8B. At high Pt loadings the situation is the opposite: the kinetic losses are reduced, because the current density per catalyst area is reduced, while the mass transport losses remain the same (the dashed lines in Figure 8A overlap), leading to a situation where the total overpotential mostly corresponds to the mass transport losses.

These observations are important not only for practical catalyst optimization, where better HER performance can be obtained both by more active catalysts or higher catalyst loading, but also for mechanistic studies that aim to identify different reaction mechanisms on the basis of their different Tafel slopes. We can see this in Figure 8A, where the (Tafel) slope of the curves change significantly when going from kinetics determined solely by mass transport (dashed line in Figure 8A) to the situation with negligible mass transport losses (10 ng/cm^2). This transition from mass transport control to kinetics-dominated overpotential is a likely explanation for the apparent discrepancy between the values in the literature with different Tafel slopes and exchange current densities [7,8]. Indeed, if the mass transport effects were not taken into account when considering this situation, it would appear as if the reaction mechanism changes with the catalyst loading (Figure 8A), and the kinetics become faster (overpotential smaller) with lower loadings (Figure 8B). In reality, however, the changes come from differences in the dependence of the kinetic and mass transport overpotentials on current densities per electrode and catalyst surface area.

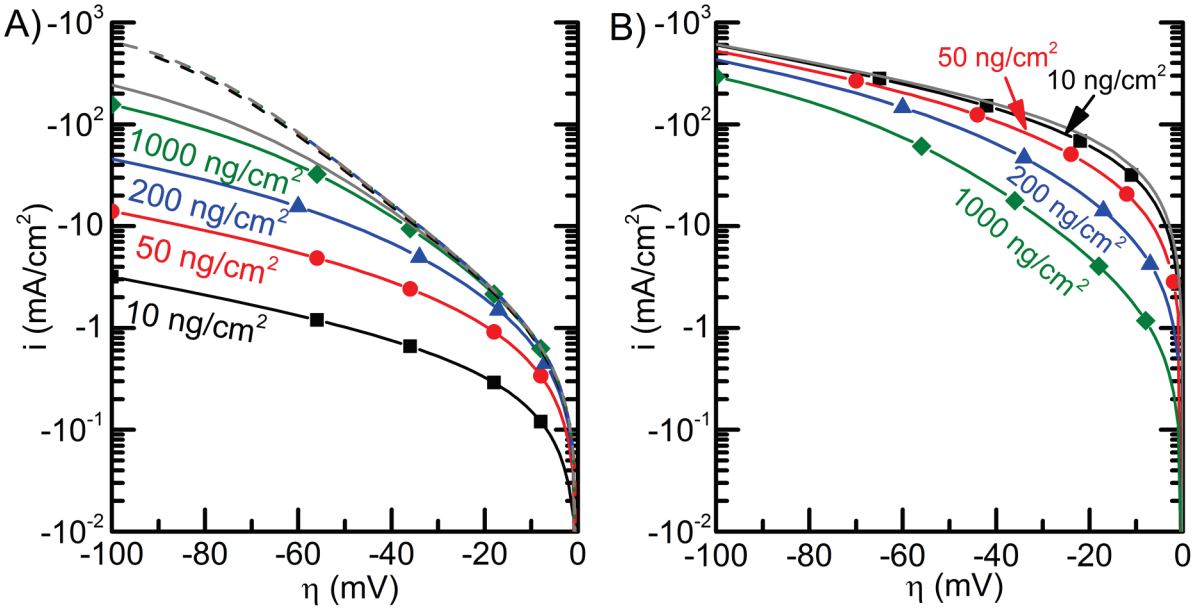

Figure 8. A) The effect of Pt loading of particles 5 nm in diameter on the IV curve of the electrode compared to flat Pt (gray). The dashed lines indicate current density as a function of mass transport overpotential. B) Current density on Pt surface compared to the theoretical limit without mass transport losses (gray).

3.3. Equilibrium coverage and Tafel slope

Detailed theoretical analysis of HER/HOR and the kinetic parameters has been carried out earlier [18,27–29]. Although we use the Langmuir adsorption isotherm instead of Frumkin, many characteristics related to the Tafel rate and equilibrium coverage are similar. However, previous analysis of the V-T route has often assumed a low equilibrium coverage, whereas here we vary it over a broad range [27,28]. We use 10 ng/cm^2 catalyst loading to illustrate the reaction kinetics, because from the loadings under study it gives the highest kinetic losses, and therefore an IV curve closest to the theoretical limit of kinetic control without mass transport losses (see Figure 8B).

Figure 9A shows the effect of the equilibrium coverage with 10 ng/cm^2 loading on the IV curve of the electrode and the other parameters kept as in Table A.1. The left-hand axis shows the current density per Pt surface area, and the right-hand axis per electrode area. When the coverage is close to the equilibrium value, the Tafel slope of the IV curve is approximately 120 mV/decade (solid gray line in Figure 9A) when Volmer is the RLS. However, the kinetics of the Tafel step dictate that in steady state the coverage increases when the current density increases, even if the surface concentrations are equal to the bulk concentrations. Therefore, in reality the change in coverage always affects the IV curve to some extent. When equilibrium coverage is low, the number of free adsorption sites decreases slowly when the current is increased and thus the effect on the overpotential is small. This yields an IV curve that is very close to the 120 mV/decade Tafel slope. However, with high equilibrium coverage, the relative change in the number of free adsorption sites is larger and the overpotential required for a given current density increases faster than 120 mV/decade. In the case of the V-T mechanism a higher equilibrium coverage also limits the highest attainable HER current density, which is seen with equilibrium coverages higher than 0.5 in Figure 9.

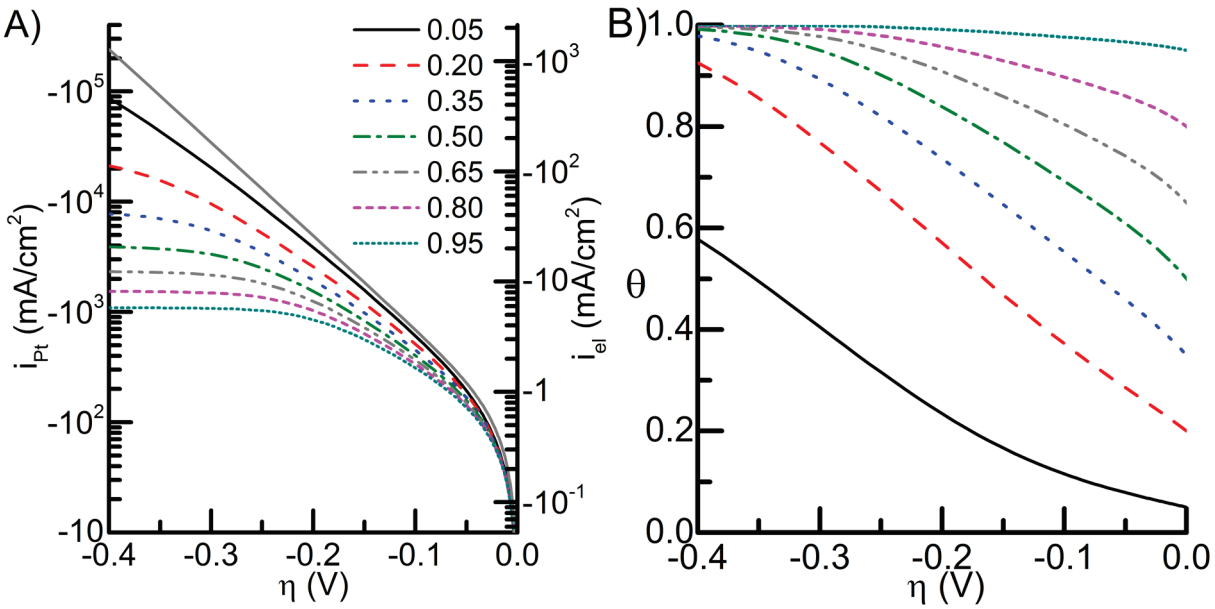

Figure 9. A) The effect of the equilibrium hydrogen coverage on the current-overpotential curve of the electrode with 10 ng/cm^2 Pt loading, represented in terms of the current density at the Pt surface (left-hand axis) and averaged over the electrode area (right-hand axis). The solid gray line corresponds to the Butler-Volmer equation with i_0 = 100 mA/cm^2 and α = 0.5 (~120 mV/decade Tafel slope). B) The hydrogen coverage of the Pt particles for the simulated equilibrium coverages.

The difference between the gray lines indicating the theoretical limits in Figures 8B and 9A is that in 8B the effect of increasing surface coverage is included, whereas in 9A the Butler-Volmer equation corresponds to a constant surface coverage to illustrate how increasing (equilibrium) coverage affects the IV curve.

4. Conclusions

Here we presented a mass transport model that can describe the H_2 transport in greater detail than the diffusion layer approach with only a single H_2 species. At low current densities the mass exchange between gaseous and dissolved H_2 molecules leads to mass transport that seems diffusive, although the origin of the apparent limiting current density is in the mass exchange kinetics. Increased gas volume enhances the kinetics, leading to faster apparent H_2 mass transport. Although the model is mainly suited to low gas concentrations and the results differ somewhat from the experimental data, it is a first step towards a realistic H_2 mass transport model for solar photoelectrolysis cells. Possible ways to improve the model were discussed, such as taking into account the bubble growth and changing surface area, and using the gas volume fraction to describe the effects of the bubble movement on diffusion in the liquid.

An important detail for the electrode and catalyst operation is that the mass transport and kinetic overpotentials depend on different current densities, the mass transport overpotential on the current per electrode area and the kinetic overpotential on the current density per catalyst surface. As we showed, this may lead to a situation where it seems that the reaction kinetics, both the exchange current density and the Tafel slope, depend on the amount of catalyst, when in fact only the relative significance of mass transport and kinetic losses has changed. Because this may lead to misinterpretations of the measurement results, especially when good catalysts are being considered, it should preferably already be taken into account in the planning phase of experiments. The model and results presented should allow more accurate estimation of the effects of mass transport, reaction kinetics and catalyst loading on the experimental results and serve as a tool for optimizing catalyst use in photoelectrolysis cells.

Acknowledgements

This work was funded by Nordic Energy Research within the Nordic Initiative for Solar Fuel Development (NISFD) project.

Appendix: The simulation parameters

The baseline simulation parameters are given in Table A.1. Some parameters are varied in the simulations, but those in the table comprise a baseline with which the other results are compared. To the best of our knowledge, the ratio of the Tafel and Volmer exchange rates (r_T) has not been determined experimentally, and several different estimates for the equilibrium coverage have been presented, ranging at least from 5% to 67% [6,18,30] and even one as low as 0.001% has been used in theoretical analysis [27]. The values in Table A.1 are thus reasonable estimates based on other results: the equilibrium coverage is based on Wang et al. [18] and the rate of the Tafel step on the fact that the reaction kinetics would have to allow at least the measured HOR current density of 500 mA/cm^2 [8]. When the Volmer exchange current density is 100 mA/cm^2 and the change in the coverage with current density is neglected,

the value of r_T would have to be at least 2.5. However, the reduction in coverage with an increasing HOR current density means that a lower ratio would be sufficient, the exact value depending on the equilibrium coverage. We chose to use a ratio that was twice as high (5.0) in the simulations.

Table A.1. Simulation parameters and their baseline case values.

Symbol	Explanation	Value
T	Temperature	298.15 K
Z_b	Thickness of the electrolyte diffusion layer	100 μm
h_{TiO_2}	Thickness of the TiO_2 layer	100 nm
σ_{TiO_2}	Conductivity of TiO_2	1 S/m
d_{Pt}	Diameter of Pt particles	5 nm
ρ_{Pt}	Density of Pt	21450 kg/m^3 [31]
σ_{Pt}	Conductivity of Pt	9.43×10^6 S/m [31]
$i_{0,V}$	Exchange current density of Volmer reaction	100 mA/cm^2 [8]
r_H	Ratio of Heyrovsky and Volmer rates	0 [8]
r_T	Ratio of Tafel and Volmer rates	5 [8]
θ^0	Equilibrium H-coverage	0.05 [18]
d_b	Diameter of H_2 bubbles	440 nm [14]
k_{diss}	H_2 dissolvation rate constant	0.4 mm/s [14]
$c^0_{H^+}$	Bulk proton concentration	1.0 M
$c^0_{H_2}$	Bulk H_2 concentration	0.07698 mM [14]
$f_g\rho^0_g$	Bulk effective density of H_2 gas	0.0015518 kg/m^3
k_{H,H_2}	Henry's law coefficient between H_2 gas and hydrated H_2	12990 bar/M
D_{H^+}	Diffusion coefficient of protons	9.3110×10^{-5} cm^2/s [31]
$D_{ClO_4^-}$	Diffusion coefficient of perchlorate ions	1.7908×10^{-5} cm^2/s [31]
D_{H_2}	Diffusion coefficient of hydrated H_2	5.1100×10^{-5} cm^2/s [31]
μ_{H^+}	Mobility of protons	3.624×10^{-3} cm^2/(V·s) [31]
$\mu_{ClO_4^-}$	Mobility of perchlorate ions	6.970×10^{-4} cm^2/(V·s) [31]

References

[1] Hu S, Xiang C, Haussener S, Berger AD, Lewis NS. An analysis of the optimal band gaps of light absorbers in integrated tandem photoelectrochemical water-splitting systems. Energy Environ Sci 2013;6:2984–93. doi:10.1039/c3ee40453f.

[2] Haussener S, Hu S, Xiang C, Weber AZ, Lewis NS. Simulations of the irradiation and temperature dependence of the efficiency of tandem photoelectrochemical water-splitting systems. Energy Environ Sci 2013;6:3604–18. doi:10.1039/c3ee41302k.

[3] Jacobsson TJ, Fjällström V, Edoff M, Edvinsson T. Sustainable solar hydrogen production: from photoelectrochemical cells to PV-electrolyzers and back again. Energy Environ Sci 2014;7:2056–70. doi:10.1039/c4ee00754a.

[4] Vesborg PCK, Seger B, Chorkendorff I. Recent Development in Hydrogen Evolution Reaction Catalysts and Their Practical Implementation. J Phys Chem Lett 2015;6:951–7. doi:10.1021/acs.jpclett.5b00306.

[5] McKone JR, Marinescu SC, Brunschwig BS, Winkler JR, Gray HB. Earth-abundant hydrogen evolution electrocatalysts. Chem Sci 2014;5:865–78. doi:10.1039/C3SC51711J.

[6] Quaino PM, Gennero de Chialvo MR, Chialvo AC. Hydrogen electrode reaction: A complete kinetic description. Electrochim Acta 2007;52:7396–403. doi:10.1016/j.electacta.2007.06.030.

[7] Neyerlin KC, Gu W, Jorne J, Gasteiger HA. Study of the Exchange Current Density for the Hydrogen Oxidation and Evolution Reactions. J Electrochem Soc 2007;154:B631–5. doi:10.1149/1.2733987.

[8] Durst J, Simon C, Gasteiger HA. Hydrogen Oxidation and Evolution Reaction Kinetics on Carbon Supported Pt, Ir, Rh, and Pd Electrocatalysts in Acidic Media. J Electrochem Soc 2015;162:F190–203. doi:10.1149/2.0981501jes.

[9] Zalitis CM, Sharman J, Wright E, Kucernak AR. Properties of the hydrogen oxidation reaction on Pt/C catalysts at optimised high mass transport conditions and its relevance to the anode reaction in PEFCs and cathode reactions in electrolysers. Electrochim Acta 2015;176:763–76. doi:10.1016/j.electacta.2015.06.146.

[10] Kemppainen E, Bodin A, Sebok B, Pedersen T, Seger BJ, Mei B, et al. Scalability and feasibility of photoelectrochemical H_2 evolution: The ultimate limit of Pt nanoparticle as an HER catalyst. Energy Environ Sci 2015;8:2991–9. doi:10.1039/C5EE02188J.

[11] Chen S, Kucernak A. Electrodeposition of Platinum on Nanometer-Sized Carbon Electrodes. J Phys Chem B 2003;107:8392–402. doi:10.1021/jp0348934.

[12] Aoki K. Theory of ultramicroelectrodes. Electroanalysis 1993;5:627–39. doi:10.1002/elan.1140050802.

[13] Bard AJ, Faulkner LR. Electrochemical Methods: Fundamentals and Applications. WILEY-VCH Verlag; 2001.

[14] Aoki K, Toda H, Yamamoto J, Chen J, Nishiumi T. Is hydrogen gas in water present as bubbles or hydrated form? J Electroanal Chem 2012;668:83–9. doi:10.1016/j.jelechem.2012.01.013.

[15] Svetovoy VB, Sanders RGP, Elwenspoek MC. Transient Nanobubbles in Short-Time Electrolysis. J Phys Condens Matter 2013;25:184002. doi:10.1088/0953-8984/25/18/184002.

[16] Janssen LJJ, Hoogland JG. The effect of electrolytically evolved gas bubbles on the thickness of the diffusion layer—II. Electrochim Acta 1973;18:543–50. doi:10.1016/0013-4686(73)85016-9.

[17] Vogt H, Stephan K. Local microprocesses at gas-evolving electrodes and their influence on mass transfer. Electrochim Acta 2015;155:348–56. doi:10.1016/j.electacta.2015.01.008.

[18] Wang JX, Springer TE, Adzic RR. Dual-Pathway Kinetic Equation for the Hydrogen Oxidation Reaction on Pt Electrodes. J Electrochem Soc 2006;153:A1732–40. doi:10.1149/1.2218756.

[19] Reller H, Kirowa-Eisner E, Gileadi E. Ensembles of Microelectrodes: A Digital Simulation. J Electroanal Chem Interfacial Electrochem 1982;138:65–77. doi:10.1016/0022-0728(82)87128-3.

[20] Compton RG, Wildgoose GG, Rees N V., Streeter I, Baron R. Design, fabrication, characterisation and application of nanoelectrode arrays. Chem Phys Lett 2008;459:1–17. doi:10.1016/j.cplett.2008.03.095.

[21] Harrison J, Khan Z. The oxidation of hydrogen. J Electroanal Chem Interfacial Electrochem 1971;30:327–30. doi:10.1016/0368-1874(71)85070-0.

[22] Manzanares JA, Kontturi K. Diffusion and migration. Encycl. Electrochem. Vol. 2, Interfacial Kinet. Mass Transp., 2003, p. 81–145.

[23] Lewis WK, Whitman WG. Principles of gas absorption. Ind Eng Chem 1924;16:1215–20.

[24] Vogt H, Balzer RJ. The bubble coverage of gas-evolving electrodes in stagnant electrolytes. Electrochim Acta 2005;50:2073–9. doi:10.1016/j.electacta.2004.09.025.

[25] Vogt H. Heat transfer in boiling and mass transfer in gas evolution at electrodes – The analogy and its limits. Int J Heat Mass Transf 2013;59:191–7. doi:10.1016/j.ijheatmasstransfer.2012.12.018.

[26] Vogt H. The actual current density of gas-evolving electrodes - Notes on the bubble coverage. Electrochim Acta 2012;78:183–7. doi:10.1016/j.electacta.2012.05.124.

[27] Gennero de Chialvo MR, Chialvo AC. Kinetics of hydrogen evolution reaction with Frumkin adsorption: re-examination of the Volmer–Heyrovsky and Volmer–Tafel routes. Electrochim Acta 1998;44:841–51. doi:10.1016/S0013-4686(98)00233-3.

[28] Gennero de Chialvo MR, Chialvo AC. Hydrogen diffusion effects on the kinetics of the hydrogen electrode reaction. Part I. Theoretical aspects. Phys Chem Chem Phys 2004;6:4009–17. doi:10.1039/b402695k.

[29] Arce MD, Bonazza HL, Fernández JL. Kinetic analysis of the hydrogen electrode reaction in unbuffered media. Theory and studies on Pt microelectrodes. Electrochim Acta 2013;107:248–60. doi:10.1016/j.electacta.2013.05.135.

[30] Markovic NM, Ross PNJ. Surface science studies of model fuel cell electrocatalysts. Surf Sci Rep 2002;45:117–229. doi:10.1016/S0167-5729(01)00022-X.

[31] Haynes WM, editor. CRC Handbook of Chemistry and Physics. 95th ed. CRC Press; 2014.